Horizontal dam-break flow past a blocking-drag region

Cite as: Phys. Fluids **34**, 052104 (2022); https://doi.org/10.1063/5.0079188
Submitted: 18 November 2021 • Accepted: 19 March 2022 • Published Online: 03 May 2022
Published open access through an agreement with JISC Collections

I. Eames and T. Robinson

Physics of Fluids ARTICLE scitation.org/journal/phf

Horizontal dam-break flow past a blocking-drag region

Cite as: Phys. Fluids **34**, 052104 (2022); doi: 10.1063/5.0079188
Submitted: 18 November 2021 · Accepted: 19 March 2022 ·
Published Online: 3 May 2022

View Online Export Citation CrossMark

I. Eames[1,a] and T. Robinson[2]

AFFILIATIONS

[1]Centre for Engineering in Extreme Environments, University College London, Gower Street, London WC1E 6BT, United Kingdom
[2]Department of Civil, Environmental and Geomatic Engineering, University College London, Gower Street, London WC1E 6BT, United Kingdom

[a]Author to whom correspondence should be addressed: i.eames@ucl.ac.uk

ABSTRACT

A one-dimensional model framework of unsteady free-surface flow through a blocking-drag region is developed, tested, and applied to understand the dam-break flow past a rectangular building. This is achieved by studying the steady-state, adjustment to steady-state, and the unsteady response of a blocking-drag region. Three steady flow regimes are identified based on the Froude number upstream and downstream of a blocking-drag region: a subcritical state, a choked state with a subcritical-supercritical transition, and a supercritical state. The interaction between a dam-break flow and a blocking-drag region can be mostly understood from the quasi-steady analysis using the variation of the Froude number with time, and comparing the upstream and downstream Froude number scatter plots against the steady curve. The force time-series depends on the height of the precursor layer and the position of the blocking-drag region relative to the lock-length. This model provides considerable insight into the types of flow characteristics observed at low/high Froude numbers and goes some way to clarifying the relationship between the drag force and the dam-break flow properties.

I. INTRODUCTION

With the recent occurrence of tsunami inundation into major urban areas (2011 Tohoku earthquake and tsunami and 2004 Great Indian Ocean Tsunami) and the totality of deaths from tsunamis in the last 20 years exceeds 200 000,[1] the attention has shifted away from wave propagation across oceans to processes that occur on land. With the revision of building codes of practice,[2,3] there has been a recognition that some of the design codes are remiss in the areas of force loading, building interactions, and how buildings are modeled within tsunami codes. Since few facilities around the world have the capability of generating very long waves, except for UCL-HR Wallingford's novel tsunami facilities,[4,5] researchers have focused on using dam-break flows as a laboratory model for studying the water surge and encroach on single model buildings[6] and idealized cities.[7]

The horizontal dam-break problem consists of an instantaneous release of stationary fluid over a horizontal surface. The usual form of this problem is the lock release case where a gate that separates initially stationary bodies of fluid is removed instantaneously, and the ensuing motion is followed in time. The dam-break problem is a fundamental part of classical fluid mechanics because it provides one of the clearest applications of the Riemann technique of scalar invariants and is included in the majority of mathematics and engineering undergraduate courses.[8,9] Notwithstanding the classical nature of the technique, it is only recently that it has been used to completely map out the case of dam-break over a precursor layer in a series of remarkable papers by Hogg and colleagues.[10,11] Though the construction technique is analytical and, in parts, requires numerical evaluation, it provides a starting point to explore other components of the dam-break flow.

Numerous papers have dealt with dam-break inundation interaction with fixed buildings. In this relatively large body of work, the studies of Arnason *et al.*[12] and Douglas and Nistor[13] are noteworthy because of the detail of the experiments and the associated 3D numerical simulations against which they were compared. Arnason's study employed a precursor layer to remove the sensitivity of the leading front of the dam-break to the surface roughness to study bore interacting with a rigid building. Since the flow configurations of these studies are quite varied, no clear picture or consensus has yet emerged from this corpus of work. Recognizing that there may be a quasi-steady component to the interaction between flow inundation and buildings, Qi *et al.*[14] studied experimentally the interaction of a steady stream

with a building in a channel and observed two states where the flow downstream was either subcritical or supercritical. This phenomenon was explained in terms of a 0D model relating upstream and downstream states through an integral formulation of the conservation of momentum.

The influence of flow restrictions from side walls and submerged mounds on channel flows have been studied extensively, mostly focusing on gradual variations.[15] The presence of mounds leads to wholly supercritical or subcritical flows, with a transitional flow characterized by a hydraulic jump;[16] this bears some similarity with the types of multiple states that we analyze in this paper, with subcritical and supercritical states along with the possibility of internal shocks. Akers and Bokhove[17] extended the analysis to include a linear contraction of the channel width with the influence of the contraction largely through the resistance caused by bottom friction. When the blocking of the flow is significant, sidewall friction becomes dominant, and the influence of blocking over the entire length of the flow region must be examined. This analysis was supported by an experimental study where a two-dimensional hydraulic shock pattern, consistent with a small blocking ratio, was studied using the model of Mach.[18] Hicks *et al.*[19] studied a one-dimensional model of dam-break flow past a smoothly varying constriction with a maximum contraction of 50 percent of the channel width. The model was based on a long-wave approximation to calculate the hydrostatic force experienced by the contraction. Agreement between the free-surface water height and measurements was good upstream of the contraction, but performed poorly downstream, possibly due to the neglect of flow separation manifested as a net force on the contraction. Kocaman and Ozmen-Cagatay[20] extended this type of analysis to include sharp-edged triangular side walls contraction and observations over the length of a narrow tank that showed the accumulation of water upstream of the obstruction. The observations were compared with a volume-of-fluid method and showed good agreement. However, the tank was left open within two obstacle lengths from the contraction, and this has an undue influence on the development of the flow.

A number of studies have started to focus on the application of 2D non-linear shallow-water models to obstructions, modeling the obstruction as a hole in the computational domain, or averaging over the influence of multiple buildings.[21,22] While the blocking effect is explicitly included in these 2D models, these models require the ground friction to be tuned to match drag with experimental observation. Part of the challenge remains to understand the parameterization required for these 2D models to capture the critical flow transitions. A clear explanation of the physical processes was missing from these studies.

The purpose of this paper is to provide a new conceptual framework to explain the interactions between an inundating free-surface flow and a rigid rectangular building, using the dam-break flow as a prototype problem. Many approaches could be adopted in this regard, such as three-dimensional simulations,[23] smoothed-particle hydrodynamics models,[24,25] two-dimensional shallow-water modeling,[26] and by laboratory experiments.[27] There are a few challenges in adopting more advanced modeling techniques, specifically, the wide parameter space is too large to enable trends and dependencies to be fully explored. The approach applied here is based on exploring the properties of a one-dimensional model that incorporates the action of an obstacle on the flow. These are blocking and drag, two processes that have quite different effects on the flow. This permits us to develop a new framework and approach to understand the interaction between a free-surface flow and a blocking-drag region.

The choice and type of one-dimensional model used in this paper are important, and we elaborate this discussion in Sec. II. The model is based on an empirical force closure with the main difference being the interpretation of the influence of blocking and the impact of a drag force on the flow. Since we make use of certain results for the shallow-water flow in the absence of the blocking-drag region, the results of Hogg[10,11] are covered in Sec. III with the focusing on the transient response at a fixed point. To build up the conceptual framework, the steady problem is first studied in great detail in Sec. IV, using a graphical solution derived from the variation of the "momentum flux" (M), as defined by Lighthill,[28] with the local Froude number. Most of the physical processes can be explained by the influence of blocking and resistive force on the flow, which simplifies the analytical treatment. This is supplemented by numerical construction techniques, which highlight different regimes in the state of the flow.

In Sec. V, transient analysis is performed to examine the adjustment of a steady stream to the presence of a blocking-drag region. This shows how the steady-state conditions are reached and how this is achieved. This relationship between the initial and final state provides the link between the dam-break flow without the blocking-drag region and with the blocking-drag region. At this point, we make a comparison with data from the study by Qi *et al.*[14] that gives confidence about the modeling approach.

Finally, in Sec. VI, the dam-break flow past a uniform blocking-drag region is analyzed. The flow behavior can be understood based on the local Froude number and the steady flow regime diagram. This naturally brings together the two themes of dam-break and quasi-steady flow past buildings.

II. ONE-DIMENSIONAL NON-LINEAR SHALLOW-WATER MODEL

The dam-break configuration studied in this paper consists of the interaction between an unsteady free-surface flow and a rectangular rigid building (length L_B and width b) in a channel (width w) shown in Fig. 1. Initially, stationary fluid (height h_0 and length L_0) is held behind a removable lock at one end of the tank. Before the lock release, there is a thin precursor layer, h_L, of water in the tank. The rectangular rigid building is positioned along the center of the flume and aligned to the incident flow. The building is placed at a distance L_b from the dam-break barrier. The subscripts "u" and "d" refer to regions upstream and downstream of the building, respectively; "f" and "b" refer to positions at the front and back of the building, respectively.

A rigid building has two effects on a flow. First, it imposes a kinematic constraint on the flow, causing it to deviate around the building. This phenomenon, known as blocking, causes the flow to speed up around or between buildings[29] and has implications for the formation of hydraulic jumps and transitional flows. Second, in a steady viscous flow, rigid bodies experience a force that leads to a net reduction in the momentum flux of the flow.[30] When the flow has a free-surface, the response is more complicated because the free-surface can deform.

We adopt the term blocking-drag region to represent the rigid building, and in the model, we incorporate the effects of blocking and drag that are both dependent on the position x. In our idealized setup, both the blocking ratios (ϕ) are constant along the building

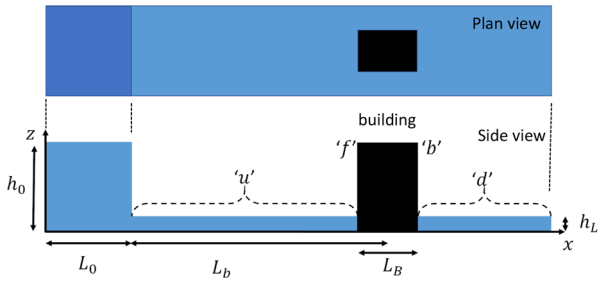

FIG. 1. A schematic of the plan and side view of the dam-break problem, at $t = 0$, with initial lock (length L_0 and height h_0), which is separated from a precursor layer of height h_L. The center of the building (length L_B) is located at a distance L_b from the front of the dam. The "*u*" and "*d*" refer regions upstream and downstream of the building, respectively. The front and the back of the building are denoted as "*f*" and "*b*," respectively.

($\phi_B = b/w$), and the drag is defined by a constant resistance coefficient C_R. However, the model is developed for a general blocking ratio $\phi(x)$ and resistance coefficient $C_T(x)$ that can vary along the tank.

A 1D approach is explored here because its simplicity permits the consequence of a building on the flow to be explored more easily and fully. This approach raises a challenge because, unlike a 2D method, the influence of a change in the blocking ratio must be modeled rather than imposed through boundary conditions applied explicitly to the flow. Simple 1D models have a role in parametric analysis in assessments of risk encapsulated in ASCE codes. A specific challenge from the 1D model comes from the blocking ratio (ϕ) being discontinuous along the channel, which means that the gradient of the blocking ratio becomes singular. There are two distinct approaches to coping with the discontinuous nature of ϕ: (1) change how the model represents the building (force closure relationship) or (2) change how the building is represented within a model (e.g., smooth ϕ). Both approaches are analyzed in this paper, but the latter approach is conceptually clearer, analytically tractable, and explains most of the physical processes.

We start the modeling discussion with concepts that will be useful for incorporating the effect of buildings into a model of the free surface flow. The first useful measure is the quantity M referred to historically as the momentum flux,[28] defined as the sum of u^2h (specific momentum flux per unit width) and $gh^2/2$ (specific pressure force per unit width). The momentum flux is a conserved quantity in the absence of an applied force. Since we are dealing with a flow in a channel with a fixed width but varying blocking ratio, these quantities are defined as

$$M = (1-\phi)\left(u^2h + \frac{1}{2}gh^2\right), \tag{1a}$$

$$q = (1-\phi)hu, \tag{1b}$$

where q is the volume flux (per unit width), and the blocking-ratio ϕ, bore height h, and the horizontal velocity u depend on the position x. For a steady free-surface flow, the change in M across a region of resistance is related to the total force (F_T) on the flow[31] through,

$$M_u - M_d = \frac{F_T}{\rho w},$$

where ρ is the fluid density and subscripts 'u' and 'd' denote upstream and downstream parameters, respectively.

Qi *et al.*[14] proposed a semi-empirical expression for the total force on a square cylinder that consisted of two distinct contributions—a resistive force and a hydrostatic force—which were parameterized in terms of the upstream and downstream flow properties as

$$F_T = \frac{1}{2}C_Q b u_u^2 h_u - \frac{1}{2}C_K \rho b g (h_u^2 - h_d^2), \tag{2}$$

where C_Q and C_K are empirical drag coefficients. The drag coefficient C_Q was estimated from the limiting case of the subcritical upstream Froude number. C_K was determined to be the best fit when the flow was choked. The value of C_Q was consistent with published measurements on square cylinders that significantly blocked the channel flow. The conclusion was that the majority of the force was largely captured by the form drag scaling.

The usual "rigorous" derivation of the non-linear shallow-water equations involves the application of a long-wave approximation and a reduction to a hydrostatic balance for pressure.[28] Expressed in a flux conserving form, the shallow-water equations describing flow over a horizontal bed are

$$\frac{\partial}{\partial t}(1-\phi)h + \frac{\partial q}{\partial x} \equiv 0, \tag{3a}$$

$$\frac{\partial q}{\partial t} + \frac{\partial M}{\partial x} = -f_T, \tag{3b}$$

where f_T is the drag force per unit length (normalized by ρw) acting on the body. The critical modeling assumption is that the influence of an obstruction can be represented by a local variation in the blocking ratio and a "distributed" resistive force. The influence of bed friction and slope can be straightforwardly incorporated into (3a) and (3b), as shown in Synolakis.[32]

Blocking and drag are quite distinct physical processes though putting an obstruction into a flow will necessarily generate both effects. The influence of blocking is implicitly included into M and q through the incorporation of the blocking ratio into the $(1-\phi)$ factor in (1a) and (1b). The drag force on an obstacle can be expressed in terms of a hydrostatic force f_H and a resistive force f_D. This distinction is not precise because the stagnation pressure caused by a flow is converted to a local water height rise/fall on the front/back face of the obstruction. This water height difference is equivalent to a hydrostatic force. Semi-empirically, we can express the drag force (per unit length, normalized by ρw) as

$$f_T = f_H + f_D,$$

the sum of the hydrostatic (f_H) and resistive force (f_D). The physical interpretation of the terms in the shallow-water models provides some guidance about which terms will be altered when the channel width varies quickly. Rewriting the shallow-water equations in a conservative form, for flow over a horizontal bed, the term on the right-hand side of the conservation of momentum (3b) is $(1/2)gh^2\partial\phi/\partial x$. The physical interpretation of this term is as the hydrostatic force (per unit length) on the channel walls as the width changes. When the change in the channel width is neither slow nor small, we would anticipate that the hydrostatic force (per unit length) to scale with $(1/2)gh^2\partial\phi/\partial x$ is of the form

$$f_H = \frac{1}{2} C_H g h^2 \frac{\partial \phi}{\partial x}, \tag{4}$$

where C_H is an empirical constant. A non-conservative form of the momentum equation (3b) can be written as

$$\frac{\partial u}{\partial t} + u\frac{\partial u}{\partial x} = -g\frac{\partial h}{\partial x} - \frac{hg(1-C_H)}{2(1-\phi)}\frac{\partial \phi}{\partial x} - \frac{f_D}{h(1-\phi)}. \tag{5}$$

At this stage, it is worth recapping the assumptions behind (3a) and (3b). The basis of the shallow-water model is a long-wave approximation and a vertical hydrostatic balance. Blocking and drag are incorporated into the model through a change in the cross-sectional width and a parameterization of a drag force per unit length (f_T); the force per unit length is written as a linear combination of a hydrostatic (f_H) and resistive component (f_D). Missing from the above model is the influence of topography and bed friction, though both can be straightforwardly added to the momentum equation. When ϕ varies gradually, it is common to set $C_H = 1$ giving the standard conservative form of the momentum equation.[19] However, for rapidly changing blocking ratios, C_H is quite different.

A closure relationship is required for the distributed resistive force (f_D) in (5). The two major factors in this choice are where and how the force is applied. Similar discussions are covered in the literature dealing with the influence of plant and urban canopies on the atmospheric boundary-layer.[33] The force applied by a body to a fluid is through its surface pressure and viscous stresses, which must be converted to a volume average, so that it can act on the flow. Strictly speaking, integrating this contribution over a plane normal to the length of the channel generates a momentum source and sink (at the front and back of a rectangular building), with a weaker, continuous distribution caused by viscous forces on the sides of the building. Including singular distributions within an unsteady numerical model is challenging, and a more common approach is to use a distributed drag model where the resistance is smeared over a region overlapping with the position of the buildings. Distributed drag models are common across many areas of fluid mechanics such as modeling offshore turbines[34] and in the context of urban terrains, where the purpose is to understand how buildings affect the urban boundary layer.[35]

Having chosen a distributed drag approach, there are a number of possible options for the closure form for f_D. The framework of dispersed multiphase flows is based on using simple force closures to describe the influence of discrete elements on the flow, and these forces tend to be correlated with the local velocity (in the absence of the element), gradients of velocity, and local fluid acceleration.[36,37] The simplest force closure that can be adopted is a resistance force proportional to the velocity squared and the local water height expressed in the form

$$f_D = C_T\,(1-\phi)\frac{u||u||h}{w}, \tag{6}$$

where the resistance coefficient C_T depends on the position x. C_T is taken to be a constant when the local Reynolds number is high. This form of the resistance force has been used for gravity currents through emergent vegetation and obstacles;[38,39] the flows in this paper are unidirectional, so that $||u|| = u$.

First, we would like to develop a model that is valid for finite changes in a streamwise blocking ratio that matches the experiments. For a rectangular building aligned to the flow, the resistance coefficient (C_T) and blocking ratio (ϕ) are uniform over a finite length L_B, centered at $x = L_b$, see Fig. 1. This relationship can be expressed as

$$\phi(x) = \phi_B\left(H\left(x - L_b + \frac{1}{2}L_B\right) - H\left(x - L_b - \frac{1}{2}L_B\right)\right), \tag{7a}$$

$$C_T(x) = C_R\frac{\phi}{\phi_B}, \tag{7b}$$

where $H(\cdot)$ is the Heaviside step function and C_R is a constant dependent on the contraction under investigation. The configuration, (7a) and 7(b), is able to mimic flows past a rectangular building (for finite ϕ_B and large C_R), emergent vegetation (for small ϕ_B and large C_R), and changes in lateral confinement (finite ϕ_B and small C_R). The hydrostatic force is singular at the front and back of the blocking-drag region, representing both a numerical challenge for unsteady flows and a conceptual challenge because a long-wave approximation is inappropriate at the singular points.

Experimental observations[14] support the view that the subcritical flow properties and force can be largely explained without a hydrostatic force. The modeling approach explored in this paper is based on setting $C_H = 0$, which has the advantage of analytical tractability. The second modeling approach is to change the way the building is represented, by replacing ϕ (7a) with a continuous form where the blocking ratio adjusts over a short smoothing distance. The former approximation is reported in this paper, but the smooth approximation was also tested and yielded substantially the same results—this is briefly discussed in Sec. VIII.

III. DAM-BREAK FLOW WITHOUT BLOCKING-DRAG REGION

In this section, we summarize the results of a dam-break flow over a precursor layer and expand on some of the analytical results of Hogg[10] and Goater and Hogg[11] that will be used later. These results act as a reference case when the blocking-drag region is weak (or $\phi \to 0$). The defining equations are given by (3a) and 3(b) with $f_T = 0$. The water behind the gate ($h = h_0$) is located in the region $0 < x < L_0$ and beyond $x = L_0$ and $h = h_L$. We work in a dimensionless form:

$$\hat{h} = h/h_0, \quad \hat{x} = x/L_0, \quad \hat{t} = (gh_0)^{1/2}t/L_0, \quad \hat{u} = u/(gh_0)^{1/2}.$$

The Riemann method involves tracking two scalar quantities

$$\alpha = \hat{u} + 2\hat{h}^{1/2}, \tag{8a}$$

$$\beta = \hat{u} - 2\hat{h}^{1/2}, \tag{8b}$$

that are invariants along the characteristics

$$\frac{\mathrm{d}\hat{x}}{\mathrm{d}\hat{t}} = \hat{u} + \hat{h}^{1/2}, \quad \frac{\mathrm{d}\hat{x}}{\mathrm{d}\hat{t}} = \hat{u} - \hat{h}^{1/2},$$

respectively. This construction technique can be used to build-up a solution over the hodograph plane from the solution at $\hat{t} = 0$. From (8a) and (8b), $\hat{u}$ and $\hat{h}$ are then determined as

$$\hat{u} = \frac{1}{2}(\alpha + \beta), \tag{9a}$$

$$\hat{h} = \frac{1}{16}(\alpha - \beta)^2. \tag{9b}$$

The hodograph plane can be separated into different regions: simple (S_1, S_2), uniform (U_1), and complex (C_1) regions depending on whether one, both, or neither of the scalar invariants is constant. Goater and Hogg[11] showed how the solutions in the various regions are constructed; for our engineering approach, we must have a clearer understanding of the physics and the dependence of $\hat{h}$ and $\hat{u}$ on time at a fixed location.

A. Region S_1

The solution uses two pieces of information in this region: $\alpha = 2$, and the expansion fan is centered at $\hat{x} = 1$. This gives the well-known solution[10,40]

$$\hat{u} = \frac{2}{3}\left(\frac{\hat{x}-1}{\hat{t}} + 1\right), \quad \hat{h} = \frac{1}{9}\left(2 - \frac{\hat{x}-1}{\hat{t}}\right)^2,$$

and a local Froude number

$$Fr = \frac{u}{(gh)^{1/2}} = 2\frac{(\hat{x}-1)/\hat{t}+1}{2-(\hat{x}-1)/\hat{t}}.$$

At a fixed point, the Froude number decreases rapidly but remains supercritical in the region $\hat{x} > 1$. The momentum flux is written as

$$\hat{u}^2\hat{h} = \frac{4}{81}\left(\frac{\hat{x}-1}{\hat{t}} + 1\right)^2\left(2 - \frac{\hat{x}-1}{\hat{t}}\right)^2, \tag{10}$$

and is bounded by 16/81. The solution in region S_1 is matched onto those in regions U_1 and C_1 across the characteristics shown in Fig. 2.

B. Region U_1

The precursor layer leads to a bore moving with a constant (dimensionless) speed (s), so that the leading-edge ($\hat{x}_f$) of the bore moves as $\hat{x}_f = s\hat{t} + 1$ and is later caught by a simple wave. In this region, $\alpha = 2$ and $\beta = \beta_m$. The bore characteristics are well-known[10,40] and determined by the mass and momentum conservation applied at the interface of the bore and precursor layer ($\hat{h}_L = h_L/h_0$),

$$\frac{1}{16}\left(\frac{1}{2}(2+\beta_m) - s\right)(2-\beta_m)^2 = -s\hat{h}_L,$$
$$\frac{1}{2}\left(\frac{1}{16}(2-\beta_m)^2 + \hat{h}_L\right) = -\left(\frac{1}{2}(2+\beta_m) - s\right)s,$$

which together enable β_m and s to be determined. We can determine from (9) the bore height and the flow speed to be

$$\hat{u} = \frac{1}{2}(2+\beta_m), \quad \hat{h} = \frac{1}{16}(2-\beta_m)^2.$$

C. Region C_1

In this region, the non-linear partial differential equation, (5), is transformed from $\hat{u}(\hat{x},\hat{t})$ and $\hat{h}(\hat{x},\hat{t})$ to a linear partial differential equation with variables $\hat{t}(\alpha,\beta)$ and $\hat{x}(\alpha,\beta)$. By integrating along the characteristics,[41] the relationship between $\hat{t}$, $\hat{x}$ and α, β is determined as

$$\hat{t}(\alpha,\beta) = \frac{64}{((\alpha+2)(2-\beta))^{3/2}}F\left(\left[\frac{3}{2},\frac{3}{2}\right], 1, \frac{(2-\alpha)(\beta+2)}{(\alpha+2)(2-\beta)}\right),$$
$$\hat{x}(\alpha,\beta) = \hat{x}(2,\beta) + \int_2^\alpha \frac{1}{4}(\alpha+3\beta)\frac{\partial\hat{t}}{\partial\alpha}\,\mathrm{d}\alpha,$$

where $\hat{x}$ is obtained by integrating along iso-β curves and F is a hypergeometric function commonly used for solving Riemann problems. Inversion is achieved by identifying iso-contours of $\hat{x}(\alpha,\beta)$ and interpolating the solution from $\hat{t}(\alpha,\beta)$. The interface between region C_1

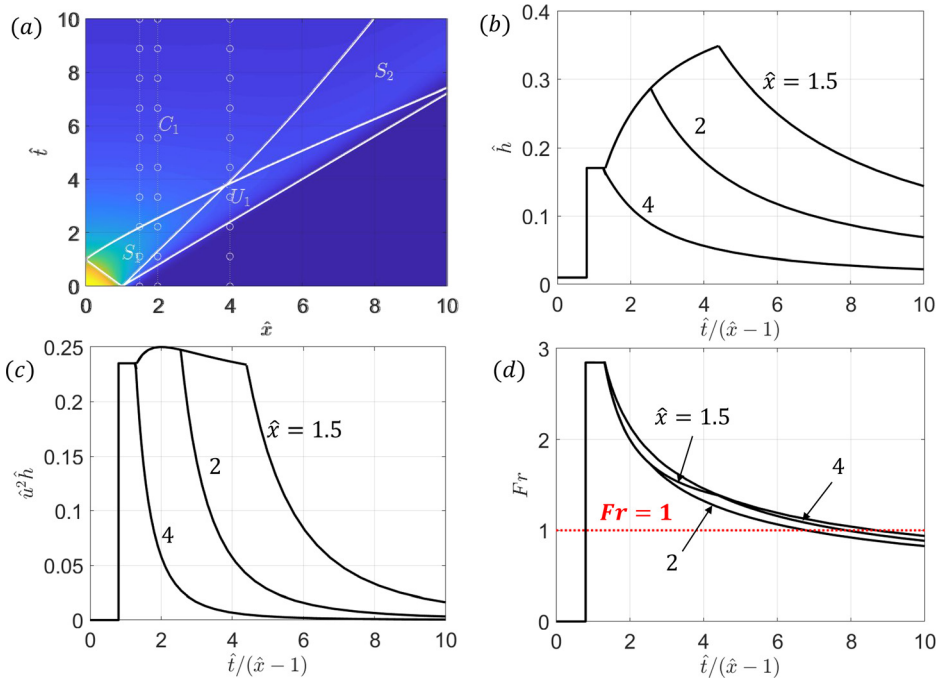

FIG. 2. Evolution of a dam-break flow with no building for $\hat{h}_L = 0.01$. In (a), the iso-contours of h are shown along with the simple $S_{1,2}$, uniform U_1, and complex C_1 regions. The superimposed vertical lines ($-o-$) represent the fixed positions $\hat{x} = 1.5$, 2, and 4. In (*b*, *c*), the water height and momentum flux are plotted as functions of time. The three curves in each plot correspond to the time histories at fixed positions $\hat{x} = 1.5$, 2, and 4. The timescale is normalized by distance between the lock gate and the fixed position ($\hat{x} - 1$), so that the different curves can be more easily distinguished of later time. The Froude number variation is shown in (d).

and S_2 is given by $\hat{x}_1(\alpha, \beta_m)$ and $\hat{t}_1(\alpha, \beta_m)$, where this region may extend quite far into the $\hat{t}$ direction where, as $\hat{t} \to \infty$, $\alpha \approx \beta \to 0$.

Looking in more detail at the singularity of F provides a good candidate for a series expansion of

$$F\left(\left[\frac{3}{2}, \frac{3}{2}\right], 1, z\right) = (1-z)^{-2}\left(1 + \frac{1}{4}z + \frac{1}{64}z^2 +, \ldots,\right). \tag{11}$$

This approximation is surprisingly good over the range $0 \le z < 1$. An asymptotic expression can be developed for time

$$\hat{t} \approx \frac{4}{(\alpha-\beta)^2}((2-\alpha)(2+\beta))^{\frac{1}{2}}\left(1 + \frac{1}{4} + \frac{1}{64} +, \ldots,\right)$$

In the limit of $\alpha, \beta \to 0$, we have manipulated (9b) using (11) to give

$$\hat{h} = \frac{1}{16}(\alpha-\beta)^2 \approx \frac{\lambda}{2\hat{t}}, \quad \lambda = 1 + \frac{1}{4} + \frac{1}{64} +, \ldots. \tag{12}$$

Hogg[42] showed that the leading coefficient $\lambda = 4/\pi$. Along the iso-β curve

$$\hat{x}(\alpha, \beta) \approx \hat{x}(2, \beta) - \lambda\left[\frac{\alpha+\beta}{2(\alpha-\beta)^2}\right]_2^{\alpha}.$$

For $\hat{h}_L \ll 1$ and large $\hat{t}$, for a fixed point,

$$\hat{x}(\alpha, \beta) \approx \hat{u}\hat{t}. \tag{13}$$

A "similarity" solution gives approximately similar results. The length of the current increases as $\hat{L} \sim 2\hat{t}$, so that the height is approximately uniform, with $\hat{h} \sim 1/\hat{L} = 1/2\hat{t}$ and a velocity $\hat{u} \sim \hat{x}/\hat{t}$. A numerical solution was developed in the limit of $\hat{h}_L \ll 1$, and similar coefficients ($\hat{h} \sim 0.55/\hat{t}$ and $\hat{u} \sim 1.06\hat{x}/\hat{t}$) were found. A detailed analysis by Hogg[42] recovers the same scaling with the leading coefficients as $\hat{h} \sim 2/\pi\hat{t}$ and $\hat{u} \sim \hat{x}/\hat{t}$.

Using (12) and (13), the solutions for the momentum flux and Froude numbers are

$$\hat{u}^2\hat{h} = \frac{\lambda}{2}\frac{\hat{x}^2}{\hat{t}^3}, \tag{14a}$$

$$Fr = \frac{2}{\lambda^{3/2}}\frac{\hat{x}}{\hat{t}^{3/2}}. \tag{14b}$$

The bore moves with speed s, and intersect region C_1 at the point

$$\hat{t}_b = \frac{8}{(2-\beta)^{3/2}}, \quad \hat{x}_b = 1 + \frac{2(2+3\beta)}{(2-\beta)^{3/2}}.$$

D. Region S_2

In region S_2, $\beta = \beta_m$ and so along the iso-α curves

$$\frac{\mathrm{d}\hat{x}}{\mathrm{d}\hat{t}} = \frac{1}{4}(3\alpha + \beta_m),$$

re-arrange as

$$\hat{t} - \hat{t}_1 = \frac{4}{3\alpha + \beta_m}(\hat{x} - \hat{x}_1),$$

hence

$$\alpha = \frac{4}{3}\left(\frac{\hat{x}-\hat{x}_1}{\hat{t}-\hat{t}_1}\right) - \frac{1}{3}\beta_m.$$

The flow properties in region S_2 are

$$\hat{u} = \frac{2}{3}\left(\frac{\hat{x}-\hat{x}_1}{\hat{t}-\hat{t}_1} + \frac{1}{2}\beta_m\right), \quad \hat{h} = \frac{1}{9}\left(\frac{\hat{x}-\hat{x}_1}{\hat{t}-\hat{t}_1} - \beta_m\right)^2.$$

Hogg constructed the solution over the whole of the hodograph plane while we proceed to focus on the part where the momentum flux is not negligible.

E. Application to three precursor heights

Figure 2 shows the solution obtained through the construction technique for a single precursor height of $\hat{h}_L = 0.01$. The results are plotted for fixed values of position but time is normalized as $\hat{t}/(\hat{x}-1)$, so that the initial time series collapse onto one curve but the later dynamics can be distinguished. The key critical observations are (1) the uniform region, U_1, gives rise to constant (supercritical flow) whose period increases as $\hat{h}_L$ increases; (2) the momentum flux ($\hat{u}^2\hat{h}$) and water height ($\hat{h}$) are constant in this region; (3) the water height and momentum flux increase in the adjacent region S_1, where the flow is supercritical. While the flow is slowing down, the water height is increasing quickly; and (4) in the region C_1, both water height and flow velocity are decreasing as the momentum flux decreases.

The first relevant point is that $\hat{u}^2\hat{h}$ varies over a smaller range than the other variables during the inundation phase. In general, $\hat{u}^2\hat{h}$ shows a weak dependence on the initial precursor height but a significant difference is in its shape. When the precursor layer is absent, the momentum flux rises smoothly before decreasing during the decay phase. Some features are retained for thin precursor layers, but the influence of the bore generates a step-change in the momentum flux.

The variation of Fr with time will be critical for our later discussion when the precursor height is small and Fr is large. The Froude number decreases rapidly because both u and $1/h^{1/2}$ decrease, but still, the flow is supercritical. The last phase is important because the water height decreases with the inverse of time, and the Froude number now becomes subcritical.

IV. STEADY FLOW PAST A BLOCKING-DRAG REGION

From Sec. III, we have seen that the water height and velocity at a fixed position may be steady for a short time (such as a precursor layer generating a bore or close to a long-dam). This indicates that the flow in the vicinity of the blocking-drag region may, under certain circumstances, also be steady. Since the steady solution ultimately underpins the transient analysis, this must be studied in detail. We do this by analyzing how the flow adjusts as it passes from upstream to downstream of the blocking-drag region. From (3a), (3b), (4), and (6), the steady flow through a blocking-drag region is governed by

$$\frac{\mathrm{d}}{\mathrm{d}x}(1-\phi)uh = 0, \tag{15a}$$

$$\frac{\mathrm{d}}{\mathrm{d}x}(1-\phi)\left(u^2h + \frac{1}{2}gh^2\right) = -\frac{1}{2}C_H g h^2\frac{\partial\phi}{\partial x} - C_T(1-\phi)\frac{u^2h}{w}. \tag{15b}$$

We can re-arrange h and u to express local variables in terms of the local Froude number,

$$h = \frac{q^{2/3} g^{-1/3} Fr^{-2/3}}{(1-\phi)^{2/3}}, \tag{16a}$$

$$u = \frac{q^{1/3} g^{1/3} Fr^{2/3}}{(1-\phi)^{1/3}}, \tag{16b}$$

where the volume flux per unit width (q) is defined in (1 b). This decomposition separates the influence of mass conservation (through q) from the momentum conservation (through Fr). Using (16a), (16b), and (15b) becomes

$$\frac{\mathrm{d}}{\mathrm{d}\tilde{x}}\left(\frac{\left(1+\frac{1}{2}Fr^{-2}\right)Fr^{2/3}}{(1-\phi)^{1/3}}\right) = \frac{1}{2}C_H \frac{\partial \phi}{\partial \tilde{x}} \frac{Fr^{-4/3}}{(1-\phi)^{4/3}} - C_T \frac{Fr^{2/3}}{(1-\phi)^{1/3}}, \tag{17}$$

here $\tilde{x} = x/w$; this can be solved by considering various parts of the flow. The dimensionless 'momentum flux' is $\hat{M}$, where

$$\hat{M} = \frac{M}{q^{4/3} g^{1/3}} = \frac{Fr^{2/3} + \frac{1}{2}Fr^{-4/3}}{(1-\phi)^{1/3}}.$$

Providing the drag force is not singular, $\hat{M}$ is a continuous in $\tilde{x}$. Upstream and downstream of the blocking-drag region and both $\hat{M}$ and Fr are constant, where

$$\hat{M}_* = Fr_*^{2/3} + \frac{1}{2}Fr_*^{-4/3},$$

where $Fr_* = u_*/(gh_*)^{1/2}$ and $*$ denotes either "u" (upstream) or "d" (downstream) regions. The total drag force caused by the blocking-drag region

$$F_T = \rho w \int_{-\infty}^{\infty} f_T \, \mathrm{d}x,$$

is evaluated by integrating $\rho w f_T$ along with the domain. From the conservation of momentum, the total drag force can also be related to the change in the momentum flux across the blocking-drag region[8,14,31] through

$$F_T = \rho w (M_u - M_d) = \rho w q^{4/3} g^{1/3} \Delta \hat{M}, \tag{18}$$

where

$$\Delta \hat{M} = \underbrace{Fr_u^{2/3} - Fr_d^{2/3}}_{\text{momentum flux}} + \underbrace{\frac{1}{2}\left(Fr_u^{-4/3} - Fr_d^{-4/3}\right)}_{\text{pressure force}}. \tag{19}$$

The total drag force can be interpreted in terms of the (actual) momentum flux or pressure force. This is important because this tells us how the flow adjusts, either through a change in water height (pressure force) or a change in velocity (momentum flux). It is useful to define an equivalent drag force coefficient (C_D) based on a representative upstream flow velocity, that is

$$C_D = \frac{2F_T}{\rho u_u^2 h_u b} = \frac{2}{\phi_B}\left(1 - \frac{Fr_d^{2/3}}{Fr_u^{2/3}}\right)\left(1 - \frac{1}{2Fr_u^{2/3}Fr_d^{4/3}}\left(1 + \frac{Fr_d^{2/3}}{Fr_u^{2/3}}\right)\right). \tag{20}$$

The peculiarity of a jump from subcritical to supercritical flow in the presence of a blocking-drag region needs to be examined using the specific energy, $E_* = u_*^2/2 + gh_*$, which represents the Bernoulli coefficient for a fluid particle on the free-surface. Ultimately, all energy is viscously dissipated but this is not explicitly accounted for in the shallow-water model and is dealt with through an implicit approach that Lighthill[28] discusses in detail through his analysis of the change in the specific energy using the example of the hydraulic jump. The specific dissipation $\Delta\Phi$ experienced by a fluid parcel is the reduction of the specific energy experienced by a fluid parcel advected across the blocking-drag region,

$$\Delta\Phi = E_u - E_d,$$

which can be expressed in a dimensionless form

$$\Delta\hat{\Phi} = \frac{\Delta\Phi}{g^{2/3}q^{2/3}} = \frac{1}{2}Fr_u^{4/3} + Fr_u^{-2/3} - \frac{1}{2}Fr_d^{4/3} - Fr_d^{-2/3},$$

and be used to discriminate whether a type of motion is permissible.

A. Uniform blocking-drag region

When the blocking ratio is a stepwise uniform and the hydrostatic force $f_H = 0$ (hence $C_H = 0$), the flow through the blocking-drag can be studied analytically. Across the front of the blocking-drag region, ϕ jumps from 0 to ϕ_B, but $\hat{M}$ is unchanged, providing a link between the Froude number upstream (Fr_u) and the Froude number at the front of the building (Fr_f), through

$$Fr_u^{2/3} + \frac{1}{2}Fr_u^{-4/3} = \frac{Fr_f^{2/3} + \frac{1}{2}Fr_f^{-4/3}}{(1-\phi_B)^{1/3}}. \tag{21}$$

Since $C_T = C_R$ and $\phi = \phi_B$ are constants within the blocking-drag region, we can integrate (17) across the length of the block to give

$$C_R \tilde{x} = \left[\frac{1}{3}\log Fr^2 - \frac{1}{3}\left(1 - \frac{1}{Fr^2}\right)\right]_{Fr_f}^{Fr_b}. \tag{22}$$

When L_B is less than the required distance for the flow to reach a critical state, Fr will vary continuously from Fr_f at the front of the blocking-drag region to Fr_b at the back of this region where [from (22)]

$$C_R \frac{L_B}{w} = \frac{1}{3}\log\frac{Fr_f^2}{Fr_b^2} + \frac{1}{3}\left(\frac{1}{Fr_f^2} - \frac{1}{Fr_b^2}\right).$$

There is a class of solutions where Fr does not vary continuously, and the flow is characterized by an internal hydraulic jump. When a stationary hydraulic jump occurs, the Froude number jumps from $Fr_+ (>1)$ to $Fr_- (<1)$ at some position within the blocking-drag region, whose location can be calculated from

$$Fr_+^{2/3} + \frac{1}{2}Fr_+^{-4/3} = Fr_-^{2/3} + \frac{1}{2}Fr_-^{-4/3},$$

$$C_R \frac{L_B}{w} = \frac{1}{3}\log\frac{Fr_f^2}{Fr_+^2} + \frac{1}{3}\log Fr_-^2 + \frac{1}{3}\left(\frac{1}{Fr_f^2} - \frac{1}{Fr_+^2} + \frac{1}{Fr_-^2} - 1\right).$$

Finally, across the end of the blocking-drag region, $\hat{M}$, is conserved, and the Froude number at the back of the region is related to the Froude number downstream through

$$\frac{Fr_b^{2/3} + \frac{1}{2}Fr_b^{-4/3}}{(1-\phi_B)^{1/3}} = Fr_d^{2/3} + \frac{1}{2}Fr_d^{-4/3}.$$

The solution can be constructed graphically from the $\hat{M}$ vs Fr plots [Figs. 3(a)–3(d)] using techniques common for Fanno flows[43] but less common for free-surface channel flows. The three possible outcomes of a steady free-surface channel flow interacting with an isolated blocking-drag region are given as cases A, B, and C. We discuss them in relation to an example of $\phi_B = 0.2$ and $C_R = 0.23$ (a value typical of a square cylinder). The variation of the water height and Froude number with distance, in the vicinity of the blocking-drag region, are shown for the cases A and B in Figs. 3(e) and 3(f).

Case A: subcritical/supercritical exchange [see Figs. 3(a) and 3(b)]. $\hat{M}$ is plotted for $\phi = 0$, corresponding to the region outside the blocking-drag region, and $\phi_B = 0.2$, corresponding to the region within the blocking-drag region. In the blocking-drag region, the resistance decreases the sum of the momentum-flux and pressure force. Upstream of the blocking-drag region, the Fr_u is constant. Across the front of the building, corresponding to a jump between "u" and "f" [shown in Fig. 3(a) and 3(b)], the cross-sectional area of the flow changes, but over a short distance, the force, $\hat{M}$, on the flow does not change. For a subcritical flow, resistance tends to increase the Froude number. When the length of the blocking-drag region is shorter than the critical distance for choking, Fr_b remains subcritical. This causes

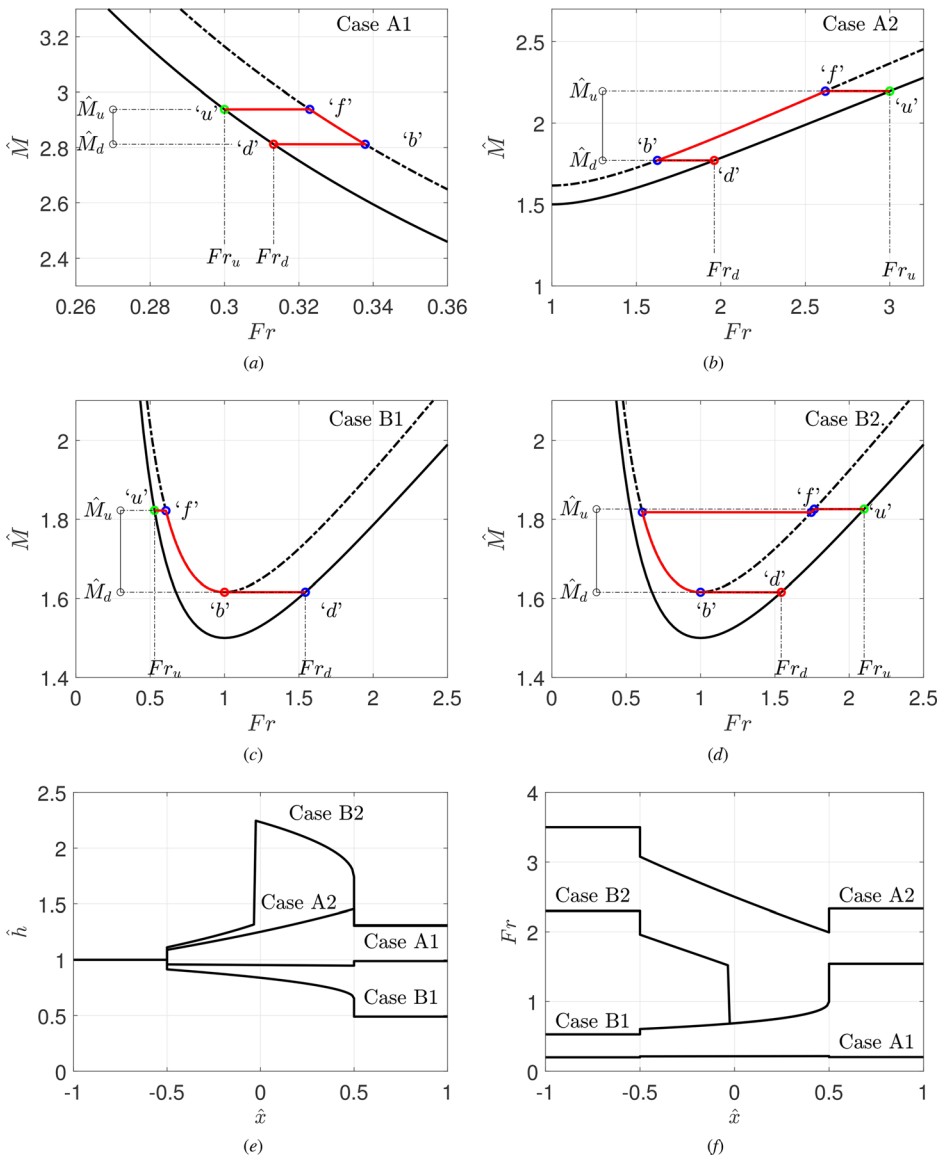

FIG. 3. Graphical interpretation of the three types of solution to the steady-state analysis obtained by looking at the variation of $\hat{M}$ with Fr for cases A1, A2, B1, and B2. In this example, $\phi_B = 0.2$ and $C_R L_B/w = 0.24$. The full ($\phi_B = 0$) and dashed $\phi_B = 0.2$ curves in (a)–(d) correspond to (4.4); they form part of the same curve but zoomed into different parts. In (a) and (b), cases A1 and A2 are shown, where a unique solution is identified and maps onto the passage from upstream through to the downstream region (for $Fr_u = 0.3, 3.0$). The variation of h and Fr with $\hat{x}$ is shown in (e) and (f), respectively.

the points to move along the momentum flux curve from "*f*" to "*b*." Finally, during the transition from position "*b*" to region "*d*," the momentum is conserved, and the solution jumps back to the initial curve. This behavior is shown for case A1, Fig. 3(a). The same explanation can be used to describe the transitional supercritical stage [case A2 Fig. 3(b)]. The corresponding height profile and local Froude number are shown in Figs. 3(e) and 3(f), respectively. For cases A1 and A2, there is a small decrease or fixed increase (of about 20%) in water height, respectively.

Case B: choked flow [see Figs. 3(c) and 3(d)]. This state corresponds to $\hat{M} = 3/2(1-\phi_B)^{1/3}$ or $Fr_b = 1$ at the back of the blocking-drag region and $Fr_d > 1$. From Fig. 3(d), we see that pure blocking does lead to a jump in the Froude number across the blocking-drag region, which is caused by the drag force. For case B1, the water height is reduced by about 40%, while for case B2, the water height is increased by 20% [as shown in Fig. 3(e)].

Case C: this region is characterized by a range of Fr_u where no solution exists to (16a) and 16(b). This is influenced by both blocking and drag. The case C is shown in Fig. 4(a) where the regime diagram for cases A, B, and C is plotted as a function of ϕ_B and Fr_u. The experimental values for the transition interface (case B) derived from the experimental observations[14,44] are shown. In addition, the horizontal lines show the intersections for $\phi_B = 0.1$, 0.2, and 0.3 and are re-plotted in Figs. 4(c) and 4(d). It is shown that largest influence, for finite ϕ, is due to blocking ratio.

Figure 4(b) shows the variation of the dimensionless total drag force, expressed in terms of the variation of $\Delta\hat{M}$ with Fr_u, where the contributions from momentum flux and pressure terms are indicated. For subcritical flows, the flow adjusts through changes in water height, rather than flow speed, while for supercritical flows, the force is primarily due to changes in the momentum flux.

When $Fr_u \ll 1$, the variation of the Froude number within the blocking-drag region is small but the change from region "*u*" to "*f*" must be taken into account, giving

$$C_{D_0} = \lim_{Fr_u \ll 1} C_D = 2C_R \frac{L_B}{b}(1-\phi_B)^{-1/2},$$

derived in limit $Fr_u \to 0$ from (21), which can be used to set C_R as

$$C_R = \frac{1}{2} C_{D_0} \frac{b}{L_B}(1-\phi_B)^{1/2}. \tag{23}$$

Similarly, when $Fr_u \gg 1$, the drag coefficient is

$$C_{D_\infty} = \lim_{Fr_u \gg 1} C_D = \frac{2}{\phi_B}\left(1 - \exp\left(-\frac{1}{2}C_{D_0}\phi_B(1-\phi_B)^{1/2}\right)\right)$$
$$\approx C_{D_0}(1-\phi_B)^{1/2},$$

where the approximation is valid for short blocking-drag regions where $C_R L_B/w < 0.2$. For the high Froude number flow, drag coefficient is, thus, reduced compared to the low Froude number limit and is close to the drag coefficient anticipated in unbounded flows. To close this problem, we need to specify the dependence of C_{D_0} on ϕ_B. Qi *et al.*[14] used the following semi-empirical closure for the drag acting on a square cylinder in a channel:

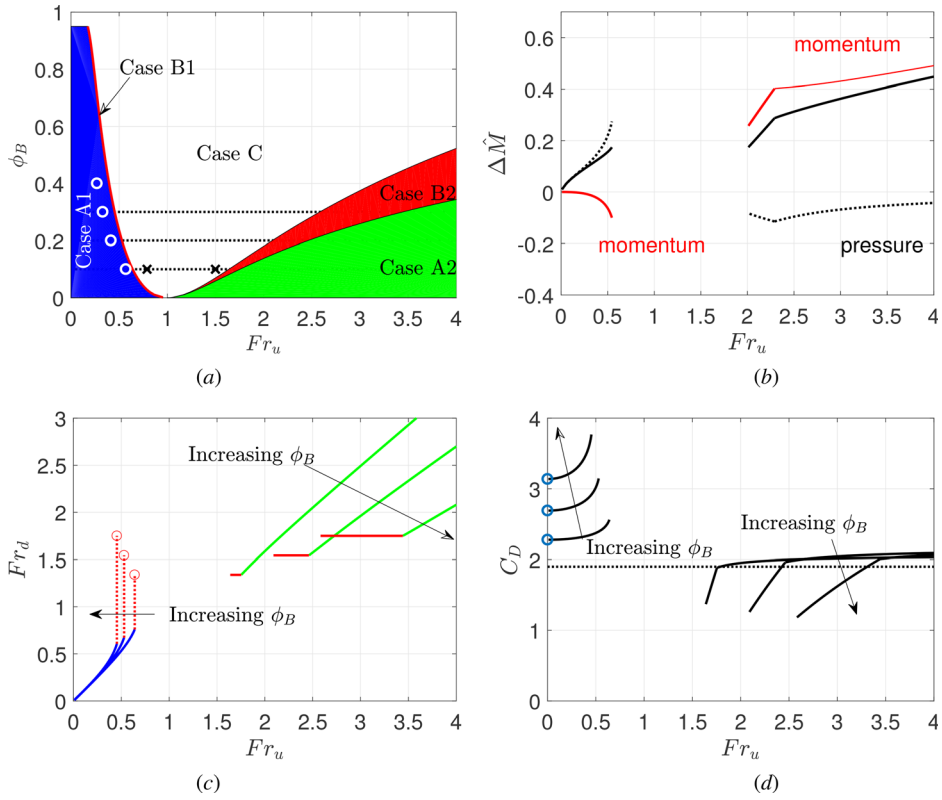

FIG. 4. In (a), a regime diagram plotted as a function of the upstream Froude number Fr_u and uniform blocking fraction ϕ_B showing the location of solutions from cases A1, A2, B1, B2, and C. The experimental results of Refs. 14 (°) and 44 (×) are shown. In (b), the change in the "momentum flux" (for $\phi_B = 0.2$) with Fr_u is shown, along with the contributions from the pressure and momentum flux terms shown in (19). In (c), the variation of Fr_d with Fr_u for $\phi_B = 0.1$, 0.2, and 0.3 is shown. The colored parts of the curves map onto the colored regions in (a). In (d), the drag coefficient C_D is shown for $\phi_B = 0.1$, 0.2, and 0.3.

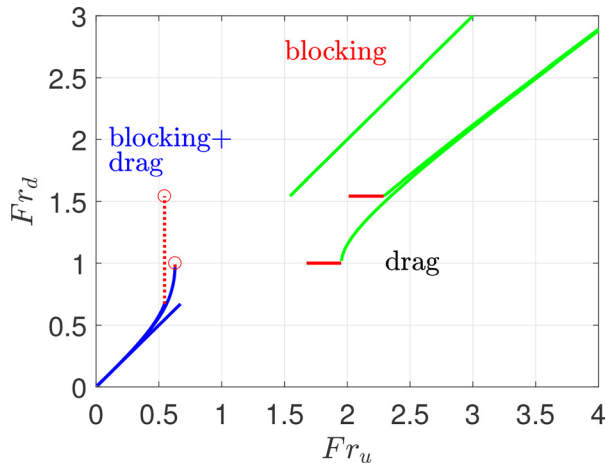

FIG. 5. The combined and separate influence of blocking and drag on the $Fr_u - Fr_d$ variation is shown for $\phi_B = 0.2$ and $C_R L_B/w = 0.24$.

$$C_{D_0} = C_0\left(1 + \frac{1}{2}C_0\phi_B\right)^2, \tag{24}$$

where $C_0 = 1.9$.

Figure 4(d) shows the variation of C_D with Fr_u, which is compared against the drag coefficient in an unbounded flow ($\phi_B = 0$) and represented by a dashed line. It shows a strong tendency of C_D to increase with Fr_u as the choked state is approached. The drag coefficient decreases dramatically for high Fr and shows a weak dependence on ϕ_B.

The separate and combined effect of blocking and drag on the regime diagram is shown in Fig. 5. Both blocking and drag tend to force a subcritical and supercritical upstream flow toward a critical state in the blocking-drag region. Case C arises because the limiting state occurs when the flow is critical at the back of the blocking-drag region leading to a gap in the Fr_u solution. The values of blocking and drag chosen in this example are typical of flow past a square obstruction where the influence of the blocking ratio is larger than the influence of the drag force.

B. Link to an integral approach or 0D model

Qi *et al.*[14] developed a 0D model based on an integral form of the conservation of momentum that relates to the reduction in the momentum flux to an empirical form of the drag force through (18) and (19). This provides a relationship between two states similar to the Rankine flow analysis of compressible flows but does not describe how the flow developed along the channel. The coefficients C_Q and C_K were chosen, so that as $Fr_u \to 0$, C_D tends to C_{D_0} which, after some manipulation, yields

$$C_Q = C_{D_0}(1 - C_K\phi_B). \tag{25}$$

Using (25), the expression (2) generates a relationship between Fr_u and Fr_d, which can be solved numerically. At the critical state, it was argued (and observed) that a transition occurred from a subcritical to a supercritical state through a hydraulic jump that was incorporated into the model.

We compare the output from the 1D and 0D models to understand how their predictive capability is related to their modeling assumptions. Figure 6 shows a comparison between the predictions from these two models for the variation of (a) the downstream Froude number, (b) drag coefficient, and (c) energy dissipation, with the upstream Froude number. Agreement for the drag force is wholly due to the fact that both models are calibrated to have the same drag coefficient as $Fr_u \to 0$.

On the subcritical branch, both modeling approaches agree closely, which is mainly due to the fact that hydrostatic forces are weak at low Fr_u [Fig. 6(a)]. The variation of the drag coefficient with Fr_u on the subcritical branches [Fig. 6(b)] is quite similar due to the calibration. Both supercritical branches indicate a general reduction in C_D at high Fr_u. We need additional information to discriminate between the different branches of the zero-dimensional model. The supercritical branch (with no solution) was argued to be nonphysical by Qi *et al.*,[14] and here, we can see that, indeed, this branch leads to a negative dissipation and can be neglected [Fig. 6(c)]. Although both supercritical and subcritical values of Fr_d are possible (when $Fr_u > 1$), the analysis shows that the subcritical branch leads to larger dissipation. Similar to the compressible flow argument for distinguishing between strong and weak oblique shocks, we could argue that the supercritical branch is favored, with the zero and one-dimensional models having similar trends.

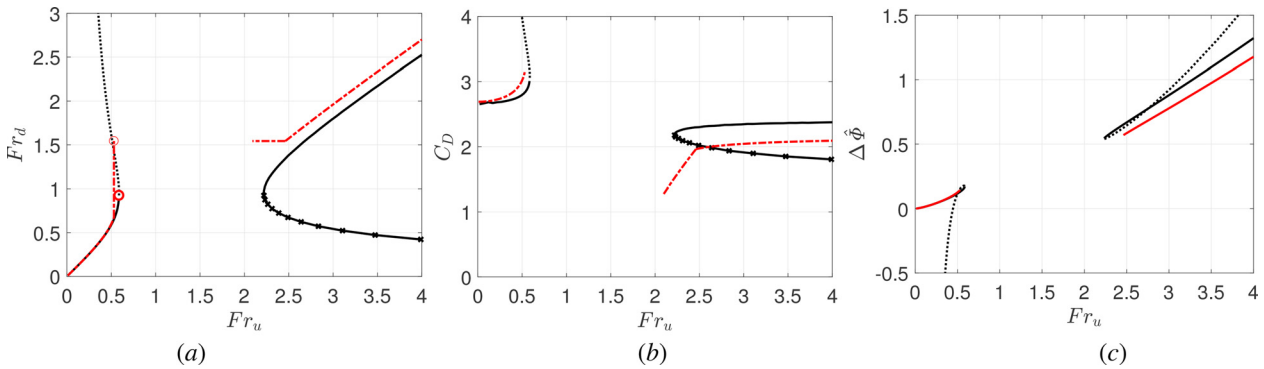

FIG. 6. Comparison between the predictions from the 0D model (black line) and 1D model (red line) for the variation of the upstream Froude number Fr_u for $\phi_B = 0.2$ with (a) the downstream Froude number Fr_d, (b) drag coefficient C_D, and (c) energy dissipation $\Delta\hat{\Phi}$. A uniform blocking ratio is taken for the one-dimensional model. The symbols on the black line are used to distinguish between the upper and lower branches in (a)–(c). The value of C_{D_0} is chosen to be the same for both 0D and 1D models.

It is worth recognizing that 1D models cannot account for upstream and downstream hydraulic jumps that are anticipated to occur for three-dimensional high Froude numbers channel flow.[45] While the model closure is based on a single value (the subcritical drag force), we would still expect the 1D model to capture the supercritical flow states and water heights because in reality, they are more strongly influenced by blocking. The presence of oblique shocks is expected to cause the downstream Froude number to be higher than the 1D predictions, and given the sensitivity of the drag to Fr_d, it is expected that the drag force to be smaller than predicted.

V. TRANSIENT RESPONSE TO A UNIFORM STREAM

We now look to see how our basic results for a steady-state flow can be used to interpret a transient flow. In this section, we consider how an initially uniform stream of water height h_0 and speed u_0, categorized with by an initial Froude number (Fr_0), adjusts in the vicinity of a blocking-drag region. To track the convergence to a steady-state, we evaluate the Froude number immediately upstream (Fr_u) and downstream (Fr_d) of the blocking-drag region. As before, we look carefully at the uniform blocking case before looking at a smoothly varying blocking ratio.

A. Final state and link to initial state

The adjustment process can be understood by writing u and h in terms of q and Fr. Substituting (16a) and 16(b) into (3a) and 3(b) gives

$$\frac{2}{3}Fr\frac{\partial q}{\partial \tilde{t}}-\frac{2}{3}q\frac{\partial Fr}{\partial \tilde{t}}+g^{1/3}q^{-1/3}Fr^{5/3}(1-\phi)^{-1/3}\frac{\partial q}{\partial \tilde{x}}=0, \tag{26a}$$

$$\begin{aligned}\frac{\partial q}{\partial t}+\frac{4}{3}q^{1/3}\frac{(1+(1/2)Fr^{-2})Fr^{2/3}g^{1/3}}{(1-\phi)^{1/3}}\frac{\partial q}{\partial \tilde{x}}&=-\frac{\partial}{\partial \tilde{x}}\frac{(1+(1/2)Fr^{-2})Fr^{2/3}}{(1-\phi)^{1/3}}-\frac{C_T}{(1-\phi)^{1/3}}Fr^{2/3}\\&\quad-\frac{1}{2}\frac{C_H}{(1-\phi)^{4/3}}Fr^{-4/3}\frac{\partial \phi}{\partial \tilde{x}}q^{4/3}g^{1/3},\end{aligned} \tag{26b}$$

where $\tilde{t}=(gh_0)^{1/2}t/L_b$. When the flow is steady ($\partial/\partial t=0$) and q is a constant term, the left-hand side of (26b) disappears, and hence, the forcing terms on the right-hand side are given as

$$\begin{aligned}0=&\underbrace{-\frac{2}{3}\frac{(Fr^2-1)Fr^{-7/3}}{(1-\phi)^{1/3}}\frac{\partial Fr}{\partial \tilde{x}}}_{\text{gradient of energy line}}\underbrace{-\frac{C_TFr^{2/3}}{(1-\phi)^{1/3}}}_{\text{drag force}}\\&\underbrace{-\frac{1}{2}\frac{C_H}{(1-\phi)^{4/3}}Fr^{-4/3}\frac{\partial \phi}{\partial \tilde{x}}}_{\text{hydrostatic force}}.\end{aligned} \tag{27}$$

The above equation retrieves (17) describing the variation of the local Froude number with distance along the channel. The sign of the forcing terms in (27) tells us how adjustment occurs when $C_H=0$. To reach an equilibrium, the first term on the right-hand side of (27) must be positive to balance the negative drag force. Therefore, for subcritical flows, Fr must be increasing with $\tilde{x}$, while for supercritical flows, Fr must be decreasing. This does not preclude the fact that the hydraulic jump might occur within the domain, and the flow switch from supercritical to subcritical, but the flow cannot be critical. When $C_H\neq 0$, since $\partial\phi/\partial\tilde{x}>0$ at the front of the blocking-drag region, the same restrictions described above apply. However, at the back of the building, where $\partial\phi/\partial\tilde{x}<0$, it is possible for there to be a jump from a supercritical state to a subcritical state over a small region.

To illustrate the adjustment process, we have chosen an example of $C_RL_B/w=0.24$, $L_B/h_0=1.0$, and $\phi_B=0.2$ to match the experimental setup of Qi *et al.*[14] While (26a) and 26(b) are written in a way to see analytically same aspects of the steady solution, the flow development was analyzed by solving (3a) and 3(b) using a constant flux and fixed water height at the inlet and zero gradients of h and uh on the outlet of the computational domain. The flow was initialized with $h=h_0$ and $u=u_0$. The simulations were applied to understand the ultimate steady-state solution using a short domain ($3L_B$) to reduce run time. The equations were solved using a standard Lax–Wendroff technique, with typically $N=1500$ points, $\delta t u_0/h_0=10^{-6}$ s, and 4×10^7 time steps; the local Courant number $\delta t|u|/\delta x$ was less than 0.01.

Ultimately, the flow tends to a steady-state, and the relationship between the upstream and downstream flow analyzed in Sec. IV is recovered, as we now confirm. Figure 7(a) shows the variation of the Fr_u, Fr_d, and Fr_0; the corresponding link between Fr_u and Fr_d is shown in Fig. 7(b). Two possible outcomes map onto the observations for the steady-state. These are

Case A: for low Fr_0 (case A1), both the upstream and downstream flows are subcritical, and the change in the Froude number across the blocking-drag regions is small. As Fr_0 increases (but remains subcritical), Fr_u increases because of a slight increase in the water height, while reversely the Fr_d increases. The main adjustment is through a weak bore propagating upstream where $Fr_u\sim Fr_0$ and $Fr_d\sim Fr_0$, until a critical Fr_0 value is reached. For case A2 (supercritical Fr_0), the adjustment comes through the propagation of a bore downstream of the blocking-drag region. The upstream Froude number remains unchanged $Fr_u=Fr_0$, and the Fr_d is smaller but supercritical.

Case B: for intermediate values of Fr_0, which crosses both subcritical and supercritical flows, the adjustment process is dramatic. This corresponds to the case where there is no steady-state solution. The upstream Froude number reaches a critical limit where the flow has no solution [case C, as shown in Fig. 7(b)]. In this region, the Froude number solution is forced to the critical points where $Fr_u\approx0.5$ for case B1 and $Fr_u\approx2.1$ for case B2. As Fr_0 increases, the water height increases in this intermediate regime.

B. Comparison with experimental observations

Qi *et al.*[14] studied experimentally the flow upstream and downstream of a square cylinder fixed in a uniform stream and the drag force that acted the cylinder. Here, a comparison is made between unpublished data collected for $\phi_B=0.2$ and the model results calculated using the semi-empirical closure (24) with a uniform blocking ratio.

The first test is the limiting value of Fr_u obtained as a function of ϕ_B, which is shown in Fig. 4(a). Qi, Eames, and Johnson[14] only identified the left-hand edge of the choked region because a supercritical upstream flow could not be achieved using their experimental setup. The edge of the regime diagram for $\phi_B=0.1$ was picked up by Ducrocq *et al.*[44] who used an inclined flow to generate an upstream supercritical flow ($Fr_u>1$). The gap in the dataset of Ducrocq *et al.*[44] corresponds to the absence of a steady solution (case C), which is

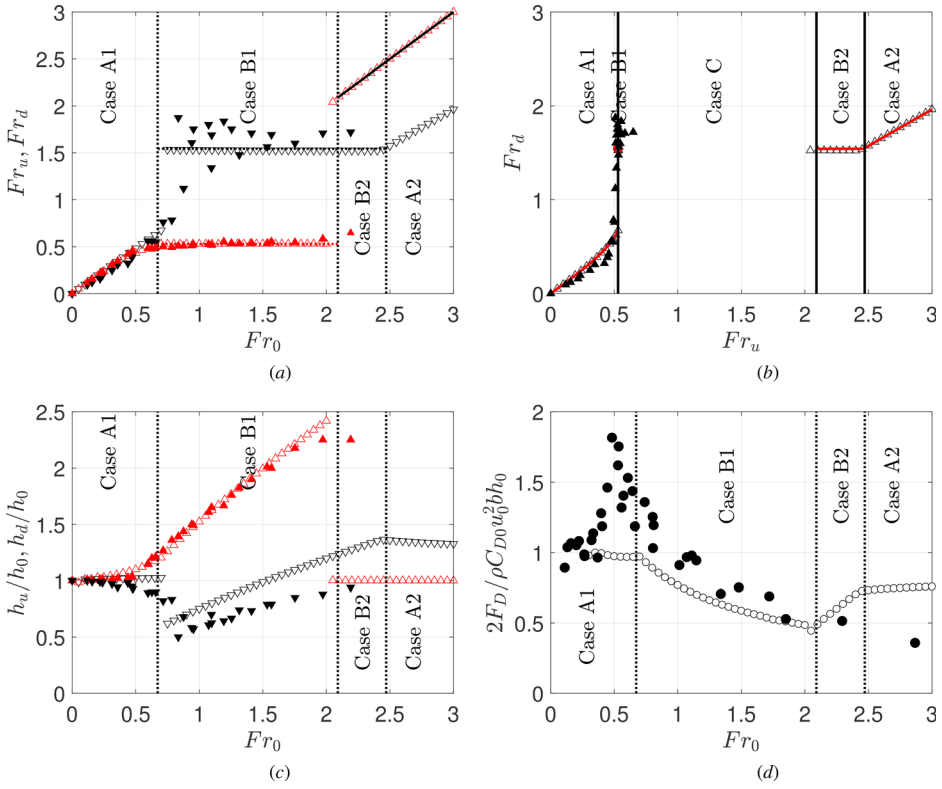

FIG. 7. The characteristics of a steady-state solution obtained from the transient analysis are compared with the experimental observations and the solution obtained from the steady-state analysis (for $\phi_B = 0.2$, $b/L_B = 1$, and $h_0/L_0 = 1$). In (a), the variation of the upstream and downstream Froude numbers is shown as a function of the initial Froude number. The vertical lines separate cases A1, B1, B2, and A2. The results from the transient analysis are plotted as △ (Fr_u) and ▽ (Fr_d), while the unpublished experimental results from Qi *et al.*[14] are plotted as full symbols (▲, ▼). The full lines are determined from the steady-state solution. In (b), Fr_d is plotted against Fr_u. The long-time solution (△) is compared with the steady-state solution (plotted as a full line and circle) and Qi *et al.*[14] (▲). The ratio of downstream and upstream water heights to the original height, determined numerically (h_u/h_0△, h_d/h_0 ▽) is shown in (c) and compared with Qi *et al.*[14] (full symbols). In (*d*), a comparison is shown between the numerically determined drag coefficient (°) and the unpublished experimental results (•).

plotted as a dashed curve bounded by two crosses in Fig. 4(a). The edge of case C is consistent with experimental observations, although there are very few studies available.

The relationship between the initial and final state can be explored in the laboratory by either dropping an obstruction into a steady stream or by characterizing the state of the flow in the absence of obstruction (to determine Fr_0). Figure 7(a) shows the variation of the upstream and downstream Froude numbers with Fr_0. During the Qi *et al.*[14] experimental study, the initial state of the Froude number and water height (Fr_0 and h_0) were noted prior to a building being introduced. A range of water heights was used but it was found that the results for water levels less than 0.04 m were susceptible to friction from the tank floor (since the tank was about 3 m long), and water heights greater than 0.15 m tended to interact with the tank ceiling when a square cylinder was introduced. The comparison was limited to having a maximum $Fr_0 < 2$ during which means that only the subcritical branch of the flow (cases A1 and B1) could be assessed. Agreement between the state of the flow characterized by the Froude number variation is good. While the 1D analysis is based on a single value of Fr_0, there is a 3D structure to the channel flow.

Figure 7(b) shows a comparison between the experimental results and the predictions for the variation of Fr_u with Fr_d for the subcritical branch, and the agreement is good. When the same experiments as Qi *et al.*[14] are repeated in a longer flume, there is sufficient distance for the hydraulic jump to be created, and the jump from the subcritical branch to choked is much more distinct. A comparison between the water heights ratios upstream and downstream of the building is shown in Fig. 7(c). Less good is the comparison between the variation in the normalized force measurement vs the initial Froude number Fig. 7(d). While agreement for $Fr_0 \to 0$ is expected because the drag coefficient used in the 1D model is semi-empirically set and the decaying trend for Fr_0 is captured, the force near the supercritical state is under-predicted. Since the 1D model does not account for the hydraulic jump that occurs downstream of the building, the increased hydrostatic force due to the water height difference on either side of the building is not accounted for. This would be the strongest candidate for explaining the under-prediction of the force. Water heights and Froude numbers are much better accounted for because they are based on height measurements and are more accurate.

VI. DAM-BREAK FLOW PAST A BLOCKING-DRAG REGION

In this section, we use the quasi-steady analysis to understand the interaction between a dam-break flow and a blocking-drag region. To simplify the message, a comparison is made with the uniform blocking case.

A. Influence of precursor layer

The dynamics of the interaction of a dam-break with a blocking-drag region can be understood through a discussion of the height profile along the flume length as a function of time. Figure 8 shows a series of snapshots corresponding to a dam-break interacting with a uniform blocking-drag region characterized by $\phi_B = 0.2$, $L_b/L_0 = 2$ and contrasting values of precursor water height ($\hat{h}_L$). The corresponding

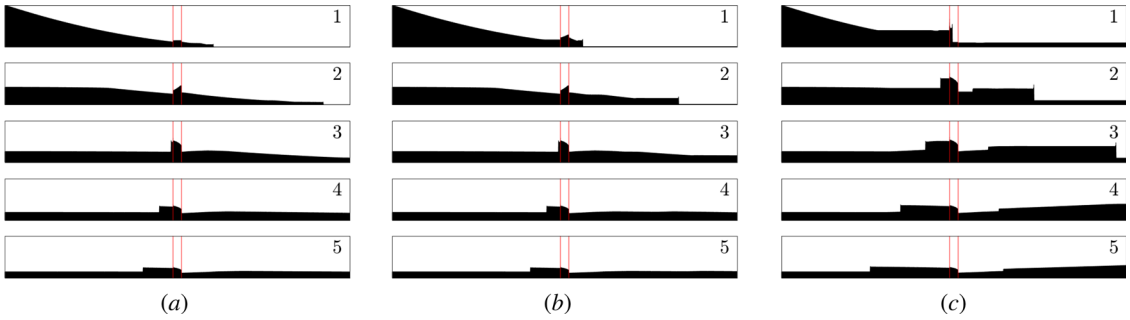

FIG. 8. Series of snap shots for the cases of dam-break where the location of the blocking-drag region is fixed at $L_b/L_0 = 2$, $\phi_B = 0.2$, $L_B/b = 1$, $h_0 = 0.4$ m, and $w = 1.0$ m. The three examples correspond to (a) $\hat{h}_L = 0.001$, (b) 0.01, and (c) 0.1. The dimensionless time for each snapshot, $\hat{t}$, is indicated on each snapshot.

changes in the Froude numbers upstream and downstream of the blocking-drag regions are shown in Fig. 9. The limits, defined from Fig. 7, of the cases A1, A2, B1, B2, and C are indicated with horizontal dashed lines in Figs. 9(a) and 9(b). For comparison, the variation of the Froude number with time in the absence of the blocking-drag region, derived using the construction technique of Sec. III, is plotted using black lines in Fig. 9(a).

When the precursor layer is thin [Fig. 8(a)], the leading-edge Froude number is much higher than the critical upstream value, and there is no initial reflection from the blocking-drag region. The upstream Froude number is initially unchanged by the presence of the blocking-drag region [Fig. 9(a)], as seen by comparing the Froude number variation plotted for the case when the body is removed—no blocking-drag region [Fig. 2(d)]. Figure 9(c) shows the Fr_d vs Fr_u trajectory whose similarity to the steady solution is demonstrated by comparing against the constructed form in Sec. IV. The arrows indicate the direction in which the trajectory moves. The upstream Froude number is compared against the case with the no blocking-drag region [Fig. 2(d)], while the downstream Froude number, Fig. 9(b), is compared against the prediction for Fr_d obtained by interpolating the curve in Fig. 7(a) using $Fr_0 = Fr_u$ determined theoretically from the upstream value. The horizontal lines in Figs. 9(a) and 9(b) correspond to the cases as seen in Fig. 7(a).

After the high Froude number interaction, Fr_d decreases, so that the $Fr_d - Fr_u$ variation collapses onto the steady analysis relationship [which is plotted in Fig. 9(c)]. The decrease in the upstream Froude number tends to bring the Froude number trajectory to the cusp of the supercritical Froude number relation and further decrease causes the trajectory to jump horizontally onto the choked state. The consequence of this jump is that the local upstream Froude number decreases and the water height increases. This creates a bore moving upstream, which can be seen in Fig. 8—the presence of the bore moving upstream was also described by Ozmen-Cagatay and Kocaman.[46] The flow is still traveling to the right but slower than the flow that is arriving at the back of the bore.

The interesting observation is that while the dynamics are significantly different for short time due to the different precursor layer thickness, the later dynamics are quite similar. Figures 10(a) and 10(b) show the influence of the precursor height on the force response, and the dash line shows the force estimate, $\frac{1}{2} C_{D_0} \hat{u}^2 \hat{h}$, where $\hat{h}$ and $\hat{u}$ are estimated from (14a), obtained from the Riemann method.

Figure 10(a) shows that the initial precursor height controls the speed of the bores, and hence, the time it takes for the flow to meet the

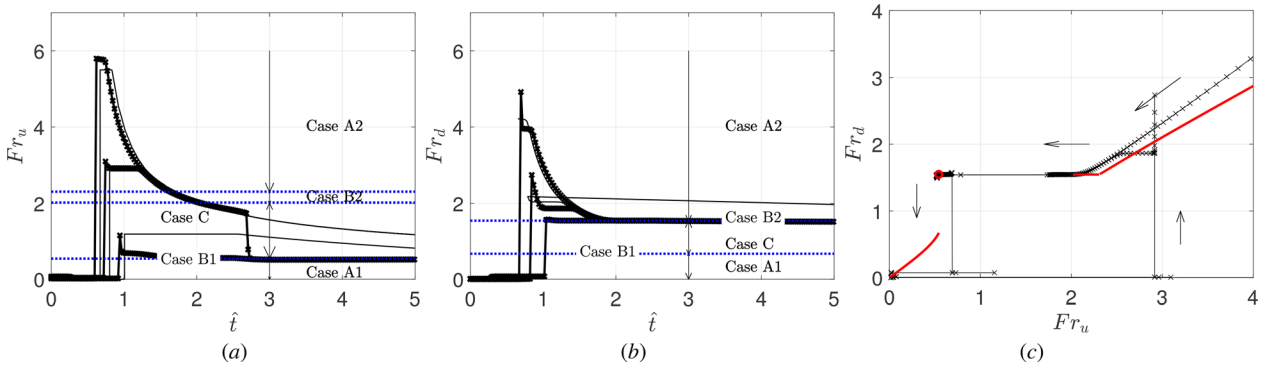

FIG. 9. The variation of the upstream and downstream Froude numbers, as a function of time, as shown for the three depths of the precursor layer. In each, $h_0 = 0.4$ m, $L_B/b = 1$, and $\phi_B = 0.2$. The center of the building is located at $L_b/L_0 = 2.0$ (where $L_0 = 2.0$ m). In (a), the thin black curve corresponds to the upstream Froude number in the absence of the blocking-drag region, while in (b), the downstream Froude number is estimated by mapping the upstream Froude number using the quasi-static estimate of $Fr_0 = Fr_u$. The lines with crosses $(- \times -)$ are the numerical results. The blue dotted lines are the fixed points of the quasi-static analysis. In (c), a scatterplot is used to map the trajectory of the $Fr_u - Fr_d$ relation for the three initial water depths. The arrows give an indication of the direction in which the trajectory moves, and the solid red line represents the quasi-static analysis.

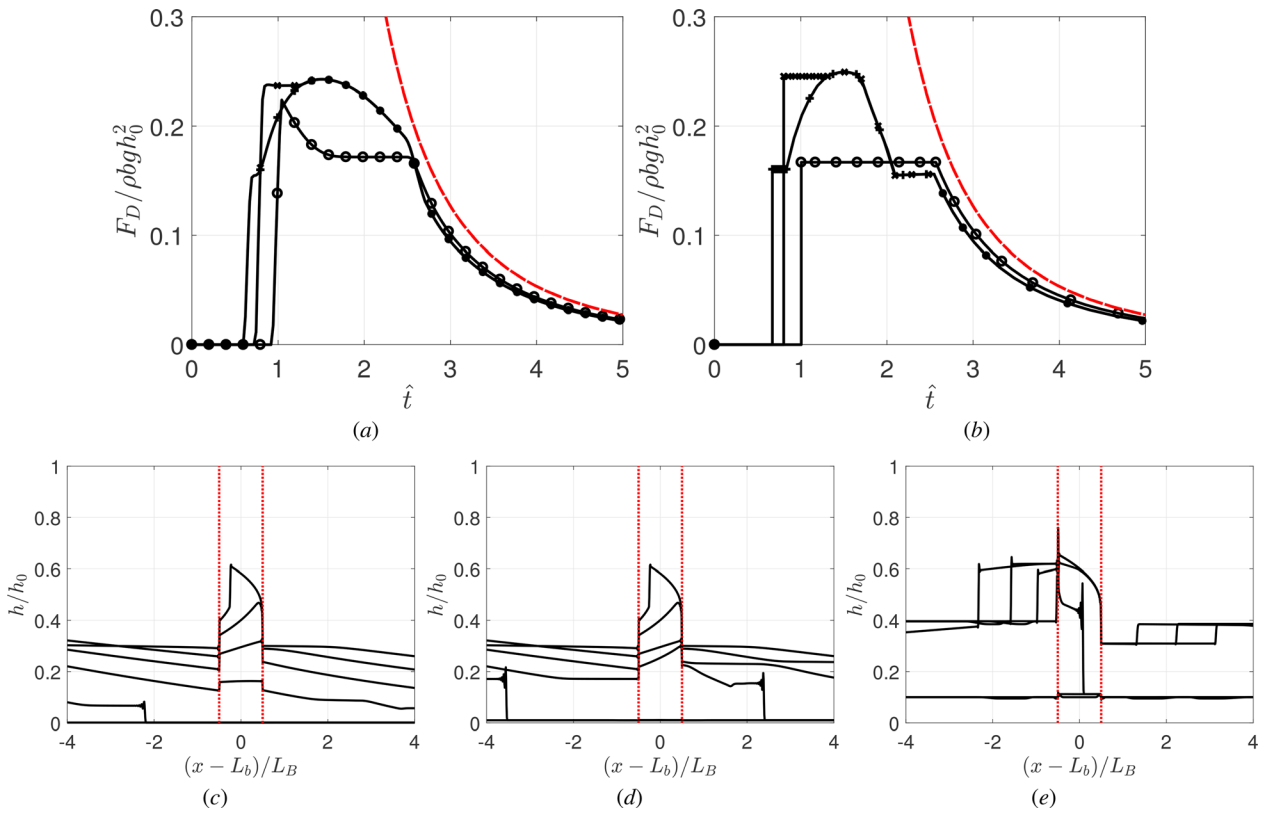

FIG. 10. The influence of the precursor thickness on force as a function of time is shown in (a) and (b) where $\hat{h}_L = 0.001$ (+), 0.01 (×), and 0.1 (°). The dashed curve corresponds to the prediction, $F_D/\rho bgh_0^2 = \frac{1}{2} C_{D_0} \hat{u}^2 \hat{h}$, where $\hat{u}^2\hat{h}$ is given by (14a). In (a), the force is determined from shallow-water equation while in (b), it is constructed from Fig. 7(d) using $Fr_0 = Fr_u$. In (c)–(e), the height profiles are shown at various time instances in the vicinity of the blocking-drag region.

blocking-drag region. The initial force response depends on the Froude number of the leading flow. For sufficiently high Fr_0, the force jumps in response to a thin bore and then rises smoothly in time [anticipated from (10) and Fig. 2(a)] in the simple wave regime before decreasing as the flow slows and the upstream water height decreases. When the initial Froude number is low, the flow rapidly switches to the choked state, leading to a sharp reduction in the drag force before tending to a constant value over the limited range of the incident bore. The timescale adjustment is long compared to the advective timescale past the blocking-drag region because the bore speed is small. As the upstream Froude number decreases, the local flow tends to become locked in the choked state.

Figure 10(b) shows the variation of the force with time estimated by taking the Froude number, in the absence of the building and calculated using the construction technique, setting $Fr_0 = Fr(t)$ to calculate F_D from Fig. 7(d). For $\hat{h}_L = 0.001$ and 0.01, the simple model largely explains the force curve, but it fails to account for the more complex adjustment that occurs for $\hat{h}_L = 0.1$. The remarkable point that the force response is so similar for later time [Figs. 10(a) and 10(b)].

Figures 10(c)–10(e) show a more detailed look at the water height in the vicinity of the blocking-drag region for the snapshots in the period prior to and after the interaction with the building. The interaction in Figs. 10(c) and 10(d) corresponds to case B2, while in Fig. 10(e), the height profile corresponds to case B1.

B. Influence of ϕ_B

The purpose of Fig. 11 is to contrast the influence of ϕ_B varying from 0.02 to 0.2 on how the state of flow, characterized by Fr_d vs Fr_u, changes. For small blocking ratios, the flow conforms closely to the steady-state analysis, with the flow ultimately jumping to the subcritical branch. As the blocking ratio increases, deeper water tends to accumulate on one side of the blocking-drag region, leading to the flow fixed at a choked state for a longer period and ultimately a lower drag ratio. For low blocking ratios, the simple model represented by the dashed curve provides a good indication of the force dynamics but misses the choked state for larger blocking ratios (Fig. 12).

C. Comparison with experimental observations

There are a few prominent experimental studies of dam-break past rigid rectangular buildings, confined in a channel. Many of these have employed large and long releases in an attempt to generate long and slow transient flows past model buildings. In principle, this provides a physical model of a bore striking a building.

The first comparison is made with Arnason,[47] who considered a variety of building shapes, including a square-based prism (oriented normal and at an angle to the incident flow) and a cylinder. Here, we compare against the square cylinder where $w = 0.6$ m, $L_b = b = 0.12$ m, and located 5.9 m from the gate. A variety of lock height releases were

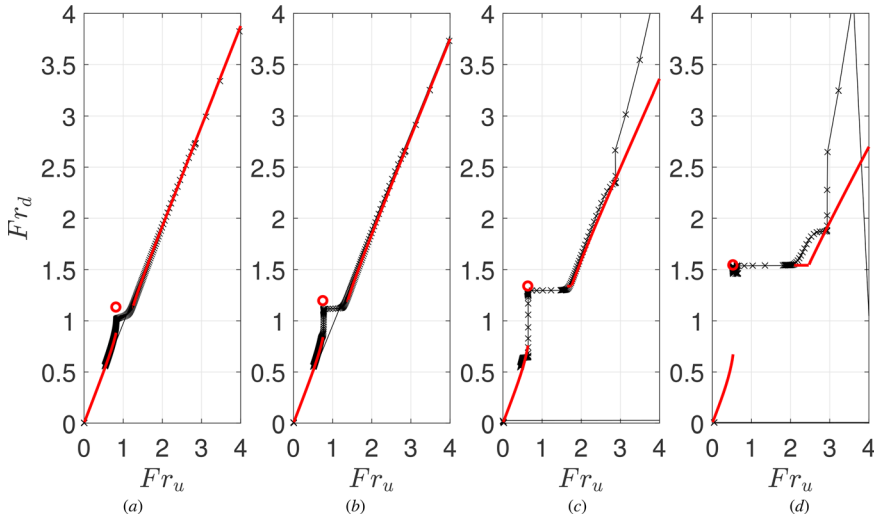

FIG. 11. Scatter plot of (Fr_d, Fr_u) for $\hat{h}_L = 0.01$, $L_b/L_B = 1.0$, $L_b/L_0 = 2.0$, and $\phi_B =$ (*a*) 0.02 (°), (*b*) 0.04 (×), (*c*) 0.1 (△), and (*d*) 0.2 (□).

considered from $h_0 = 0.1$ to 0.3 m with a lock region of length $L_0 = 5.9$ m. The simple 1D model captures the spike in the force whose origin is not related to impulsive splashing but a rapid adjustment to the choked state before tending to an approximate plateau and then a rapid decrease [Fig. 13(a)].

Nouri *et al.*[48] examined the interaction between a square column and a dam-break flow produced by the rapid opening of a gate, releasing water at a range of lock depths. The water was held in a reservoir that traveled around a 180° bend over a dry bed, leading to a high Froude number at the precursor front. We discuss their experimental results for different water heights, from the square cylinder study where $\phi_B = 0.23$. Similarly, when force tends to rise and decrease continuously before a short plateau [Fig. 13(b)]. During the steady and decaying flow regime, the square cylinder is shedding vortices, generating an unsteady drag force, which is reflected in the experimental measurements. The 1D model shows a similar peak force to the experiments, but a faster relaxation was computed, which is likely due to the significant bend on the channel. Overall agreement is good, given the simplicity of the model and is comparable to reported CFD calculations.

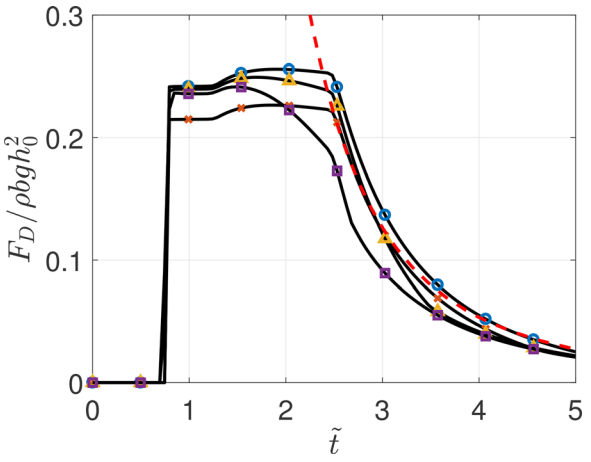

FIG. 12. The variation of the dimensionless force as a function of $\tilde{t}$ is shown for $\phi_B = 0.02$ (°), 0.04 (×), 0.1 (△), and 0.2 (□). The dotted curve corresponds to the limit of $\phi_B \to 0$, while the dashed curve is $F_D/\rho bgh_0^2 = \frac{1}{2} C_{D_0} \hat{u}^2 \hat{h}$, where $\hat{u}^2\hat{h}$ is given by (14a).

VII. CONCLUSION

In this paper, we set down a framework to analyze the interaction between a free-surface flow and a region of blocking-drag. The novelty comes from the use of a one-dimensional model of shallow-water flow to examine the distinct effects of blocking and drag on the state of the flow. We have gone into considerable detail about the steady-state solutions (cases A, B, and C). Similar types of steady-state solutions have been identified in other free-surface flows, for instance, generated by submerged mounds, bottom friction in wide channels, though the significance of sidewall drag force was not analyzed in this context. The simplest cases are where the flow is wholly subcritical or supercritical (cases A1 and A2). The flow has a critical state where there is a switch between subcritical upstream and supercritical downstream (case B1—choked state). This state is crucial to understanding the influence of the large-blocking ratio on unsteady free-surface flows. For the intermediate state, case B2, the flow adjusts from supercritical to the subcritical state through the formation of an internal hydraulic jump. There is a range of upstream Froude numbers, for which there is no steady solution (case C). The physics of these processes has been explained using a $\hat{M} - Fr$ relationship that accounts for the effect of blocking and drag. The limited available experimental data supports cases A1, B1, and C.

The steady-state analysis proved fruitful when interpreting the transient solution where we related the Froude number prior to adjustment, to the steady-state solution. The limiting steady-state results have been compared with data obtained by Qi *et al.*[14] The comparison shows that while the critical Froude numbers and water height are well predicted, the drag force near the choked state is under predicted. When the blocking ratio varies smoothly, the effect including a hydrostatic force (with $C_H = 0.2$) slightly improves the agreement of the

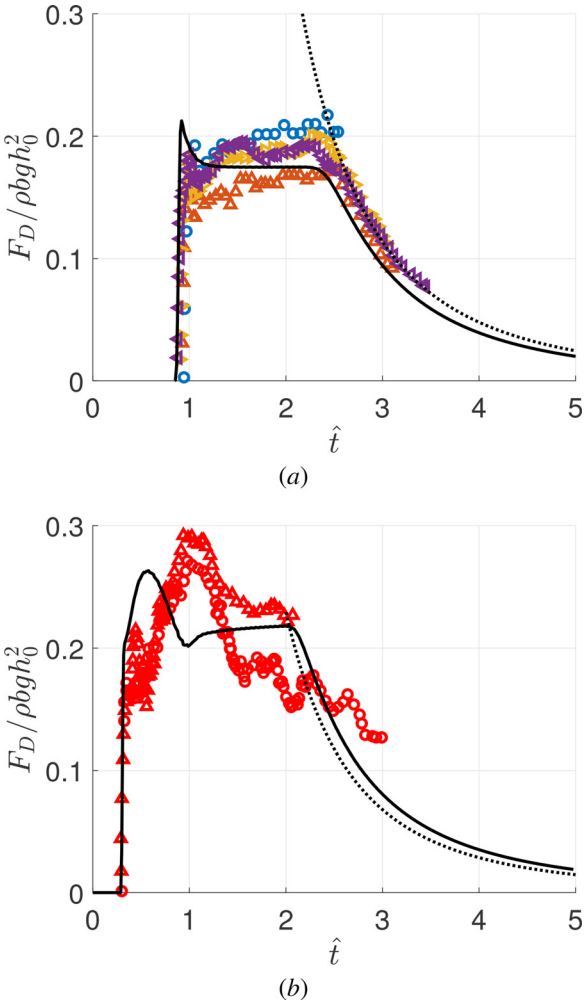

FIG. 13. A comparison is made between the model prediction for force, using the uniform blocking ratio model, and the experimental results of (a) Arnason[47] and (b) Nouri *et al.*[48] The dashed curve corresponds to the analytical prediction $F_D/\rho bgh_0^2 = \frac{1}{2} C_{D_0} \hat{u}^2 \hat{h}$ (where $\hat{u}^2\hat{h}$ is given by (14a)).

critical upstream Froude numbers and the drag coefficient close to the choked state, but otherwise, the key results are retained.

We applied the new framework to analyze the interaction between a dam-break flow and an isolated square building, which was represented as a region of uniform blocking and drag. By tracking the Froude number trajectory (based on the upstream and downstream values), we were able to identify how the transient solution closely followed the steady-state flow characteristics. The analysis identified that the flow jumped from case A2 to B2 and then across to case B1. When the upstream Froude number had dropped sufficiently, the flow jumped to the subcritical state (case A1). A comparison was made between the unsteady force calculated with the model and predictions based on combining the Froude number in the absence of the blocking-drag region with a steady analysis. Agreement was good, highlighting the importance of the steady-state analysis in explaining the underlying physical principles. A comparison was made between the drag on a square building in a dam-break flow, measured by Arnason,[47] Nouri *et al.*,[48] and the model predictions, and again, the agreement is good. The form of the drag force time series is sensitive to the depth of the precursor layer, and the difference between these two studies can be explained by the initial Froude number values.

The new framework provides a means of analyzing and understanding the profound influence of blocking and drag on unsteady free-surface flows. This has the potential to help interpret the extensive number of two- and three-dimensional simulations of free-surface flows interacting with buildings and provide guidance on flow behavior for more complex and realistic scenarios. Although the 1D model does not include the significant flow changes that occur in the vicinity of an obstruction, 3D effects such as recirculation, or 2D effects such as shock diamonds, which all contribute to a persistent downstream flow signature, the model is based on an integral form of the momentum equation and is expected to capture the gross characteristics encapsulated by the regime diagrams. Our next step is to test this framework against 2D and 3D numerical simulations, which will be reported in a later publication.

ACKNOWLEDGMENTS

I.E. and T.R. gratefully acknowledge support from the European Research Council project "URBANWAVES" (Starting Grant No. 336084) led by Professor Tiziana Rossetto. We would like to thank the referees for giving some excellent comments and providing such detailed reviews of this work. This has added clarity to the paper.

AUTHOR DECLARATIONS

Conflict of Interest

The authors have no conflicts to disclose.

DATA AVAILABILITY

The data that support the findings of this study are available from the corresponding author upon reasonable request.

REFERENCES

[1]CRED, "Economic Losses, Poverty and Disasters 1998-2017," (Centre for Research on Epidemiology of Disasters (CRED) and United Nations Office for Disaster Risk Reduction (UNISDR), 2018).
[2]American Society of Civil Engineers, "Minimum design loads for buildings and other structures," ASCE Standard No. ASCE/SEI 7-10 (American Society of Civil Engineers, Reston, Virginia, 1988).
[3]FEMA, "Guidelines for Designof Structures forVertical Evacuation from Tsunamis," Report No. FEMA P-646 (Applied Technology Council for the Federal Emergency Management Agency, Washington, D.C., 2019).
[4]T. Rossetto, W. Allsop, I. Charvet, and D. Robinson, "Physical modelling of tsunami using a new pneumatic wave generator," Coastal Eng. **58**, 517–527 (2011).
[5]D. McGovern, T. Robinson, I. Chandler, W. Allsop, and T. Rossetto, "Pneumatic long-wave generation of tsunami-length waveforms and their run-up," Coastal Eng. J. **138**, 80–97 (2018).
[6]T. Al-Faesly, D. Palermo, I. Nistor, and A. Cornett, "Experimental modeling of extreme hydrodynamic forces on structural models," Int. J. Prot. Struct. **3**(4), 477–505 (2012).
[7]S. Soares-Frazão and Y. Zech, "Dam-break flow through an idealised city," J. Hydraul. Res. **46**, 648–658 (2008).
[8]B. Massey and J. Ward-Smith, *Mechanics of Fluids*, 9th ed. (Routledge, 2012).

[9]G. Whitham, *Linear and Nonlinear Waves* (John Wiley and Sons, New York, 2011).
[10]A. Hogg, "Lock-release gravity currents and dam-break flows," J. Fluid Mech. **569**, 61–87 (2006).
[11]A. Goater and A. Hogg, "Bounded dam-break flows with tailwaters," J. Fluid Mech. **686**, 160–186 (2011).
[12]H. Arnason, C. Petroff, and H. Yeh, "Tsunami bore impingement onto a vertical column," J. Disaster Res. **4**(6), 391–403 (2009).
[13]S. Douglas and I. Nistor, "On the effect of bed condition on the development of tsunami-induced loading on structures using OpenFOAM," Nat. Hazards **76**, 1335–1356 (2015).
[14]Z. Qi, I. Eames, and E. Johnson, "Force acting on a square cylinder fixed in a free-surface channel flow," J. Fluid Mech. **756**, 716–727 (2014).
[15]C. Bellos, V. Soulis, and J. Sakkas, "Experimental investigation of two-dimensional dam-break induced flows," J. Hydraul. Res. **30**(1), 47–63 (1992).
[16]B. Baines and J. Whitehead, "On multiple states in single-layer flows," Phys. Fluids **15**, 298–307 (2003).
[17]B. Akers and O. Bokhove, "Hydraulic flow through a channel contraction: Multiple steady states," Phys. Fluids **20**, 056601 (2002).
[18]H. Reichenbach, "Contributions of Ernst mach to fluid mechanics," Annu. Rev. Fluid Mech. **15**, 1–29 (1983).
[19]F. Hicks, P. Steffler, and N. Yasmin, "One-dimensional dam-break solutions for variable width channels," J. Hydraul. Eng. **123**, 464–468 (1997).
[20]S. Kocaman and H. Ozmen-Cagatay, "The effect of lateral channel contraction on dam break flows: Laboratory experiment," J. Hydrol. **432–433**, 145–153 (2012).
[21]V. Guinot, B. Sanders, and J. Schubert, "Dual integral porosity shallow water model for urban flood modelling," Adv. Water Res. **103**, 16–31 (2017).
[22]X. Qin, M. Motley, R. LeVeque, F. Gonzalez, and K. Mueller, "A comparison of a two-dimensional depth-averaged flow model and a three-dimensional RANS model for predicting tsunami inundation and fluid forces," Nat. Hazards Earth Syst. Sci. **18**, 2489–2506 (2018).
[23]F. Aureli, S. Dazzi, A. Maranzoni, P. Mignosa, and R. Vacondio, "Experimental and numerical evaluation of the force due to the impact of a dam-break wave on a structure," Adv. Water Res. **76**, 29–42 (2015).
[24]P. St-Germain, I. Nistor, and R. Townsend, "Numerical modeling of the impact with structures of tsunami bores propagating on dry and wet beds using the SPH method," Int. J. Prot. Struct. **3**, 221–256 (2012).
[25]Z. Wei, R. Dalrymple, A. Herault, G. Bilotta, E. Rustico, and H. Yeh, "SPH modelling of dynamic impact of tsunami bore on bridge pier," Coastal Eng. **104**, 26–42 (2015).
[26]Y. Wang, Q. Liang, G. Kesserwani, and J. Hall, "A 2D shallow flow model for practical dam-break simulations," J. Hydraul. Res. **49**, 307–316 (2011).
[27]Lobovský, E. Botia-Vera, F. Castellana, J. Mas-Soler, and A. Souto-Iglesias, "Experimental investigation of dynamic pressure loads during dam break," J. Fluids Struct. **48**, 407 (2014).
[28]M. Lighthill, *Waves in Fluids* (Cambridge University Press, 1967).
[29]J. Hunt, "Oa theory of turbulent flow round two-dimensional bluff bodies," J. Fluid Mech. **61**, 625–706 (1973).
[30]A. Betz and D. G. Randall, *Introduction to the Theory of Flow Machines* (Pergamon Press, Oxford, 1966).
[31]T. Benjamin, "On the flow in channels when rigid obstacles are placed in a stream," J. Fluid Mech. **1**, 227–248 (1956).
[32]C. Synolakis, "A 2D shallow flow model for practical dam-break simulations," J. Fluid Mech. **185**, 523–545 (1987).
[33]S. Belcher, I. Harman, and J. Finnigan, "The wind in the willows: Flows in forest canopies in complex terrain," Annu. Rev. Fluid Mech. **44**, 479–504 (2012).
[34]D. Coles, L. Blunden, and A. Bahaj, "Experimental validation of the distributed drag method for simulating large marine current turbine arrays using porous fences," Int. J. Mar. Energy. **16**, 298–316 (2016).
[35]S. Belcher, N. Jerram, J. Hunt, P. Bagchi, and S. Balachandar, "Adjustment of a turbulent boundary layer to a canopy of roughness elements," J. Fluid Mech. **488**, 369–398 (2003).
[36]P. Bagchi and S. Balachandar, "Effect of turbulence on the drag and lift of a particle," Phys. Fluids **15**, 3496 (2003).
[37]J. Magnaudet and I. Eames, "The motion of high-Reynolds-number bubbles in inhomogeneous flows," Annu. Rev. Fluid Mech. **32**, 659–708 (2000).
[38]L. Hatcher, A. Hogg, and A. Woods, "The effects of drag on turbulent gravity currents," J. Fluid Mech. **416**, 297–314 (2000).
[39]H. Nepf, "Flow and transport in regions with aquatic vegetation," Annu. Rev. Fluid Mech. **44**, 123–142 (2012).
[40]J. J. Stoker, "The formation of breakers and bores the theory of nonlinear wave propagation in shallow-water and open channels," Commun. Pure Appl. Math. **1**, 1–87 (1948).
[41]P. Garabedian, *Partial Differential Equations* (Chelsea Publishing, 1986).
[42]A. Hogg, "Two-dimensional granular slumps," Phys. Fluids. **19**, 093301 (2007).
[43]J. Anderson, *Modern Compressible Flow: With Historical Perspective*, 3rd ed. (McGraw-Hill Education Europe, 2002), pp. 363–393.
[44]T. Ducrocq, L. Cassan, J. Chorda, and H. Roux, "Flow and drag force around a free surface piercing cylinder for environmental applications," Environ. Fluid Mech. **17**, 629–645 (2017).
[45]N. Riviere, G. Vouaillat, G. Launay, and E. Mignot, "Emerging obstacles in supercritical open-channel flows: Detached hydraulic jump versus wall-jet-like bow wave," J. Hydraul. Eng. **143**, 04017011 (2017).
[46]H. Ozmen-Cagatay and S. Kocaman, "Investigation of dam-break flow over abruptly contracting channel with trapezoidal-shaped lateral obstacles," J. Fluids Eng. **134**, 081204 (2012).
[47]H. Arnason, "Interactions between an incident bore and a free-standing coastal structure," Ph.D. thesis (University of Washington, Seattle, WA, 2005).
[48]Y. Nouri, I. Nistor, D. Palermo, and A. Cornett, "Experimental investigation of tsunami impact on free standing structures," Coastal Eng. **52**, 43–70 (2010).